The strain of CuO_2 lattice: the second variable for the phase diagram of cuprate perovskites

2003 J. Phys. A: Math. Gen. 36 9133

(http://iopscience.iop.org/0305-4470/36/35/302)

INSTITUTE OF PHYSICS PUBLISHING JOURNAL OF PHYSICS A: MATHEMATICAL AND GENERAL

J. Phys. A: Math. Gen. **36** (2003) 9133–9142 PII: S0305-4470(03)63692-9

The strain of CuO_2 lattice: the second variable for the phase diagram of cuprate perovskites

S Agrestini, N L Saini, G Bianconi[1] and A Bianconi

Department of Physics and INFM Unit, University of Rome 'La Sapienza', P. le A Moro 2, 00185 Roma, Italy

Received 21 May 2003
Published 20 August 2003
Online at stacks.iop.org/JPhysA/36/9133

Abstract

We show the key role of the elastic local strain (or micro-strain) ε of the CuO_2 lattice in the phase diagram of cuprate superconductors. The superconducting critical temperature $T_c(\delta, \varepsilon)$ is shown to be a function of two variables, the doping δ and the microstrain ε.

PACS number: 74.72.−h

(Some figures in this article are in colour only in the electronic version)

1. Introduction

The doped cuprate perovskites, showing high-T_c superconductivity, construct a good example of strongly correlated 2D electron phase with breakdown of the single electron picture. However, this correlated electron fluid is not a 'simple' doped 2D Mott insulator described by a single physical variable, the doping δ of the antiferromagnetic lattice (characterized by the electron–electron repulsion U, magnetic interaction J and electron transfer t). Indeed, the doping induces holes in the oxygen ($O^{2-} \rightarrow O^{1-}$, or $O(2p^6) \rightarrow O(2p^5)$) of the CuO_2 sublattice forming $Cu(3d^9)O(2p^5)$ two hole states instead of Cu^{3+} ions with $Cu(3d^8)$ two hole states in the magnetic $Cu^{2+}(3d^9)$ sublattice [1]. Therefore, localized electronic states, mostly on the Cu 3d orbitals (giving spin fluctuations), are mixed with delocalized states on the O 2p orbitals (giving a broken Fermi surface).

Here we show that the phase diagram of the electronic phase of cuprates is not simply described by a single variable: the doping δ, i.e., the number of holes per Cu site, measuring the distance from the charge transfer Mott insulator at $\delta = 0$. In fact, the curves of the superconducting critical temperature $T_c(\delta)$ versus doping are 'material dependent' as shown in figure 1.

The aim of the present work is to show that understanding the 'material dependence' of T_c via the identification of the physical variable tuned by changing the material for a constant

[1] Present address: Department de Physique, Université de Fribourg, Perolles, CH-1700 Switzerland.

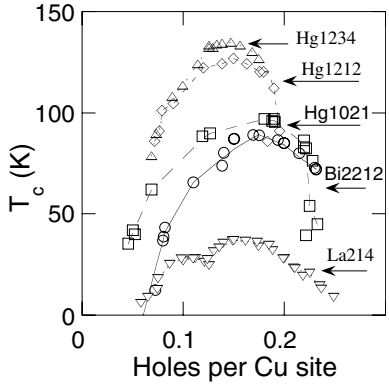

Figure 1. The experimental curves of the superconducting critical temperature T_c versus the hole doping δ in different cuprate perovskite families.

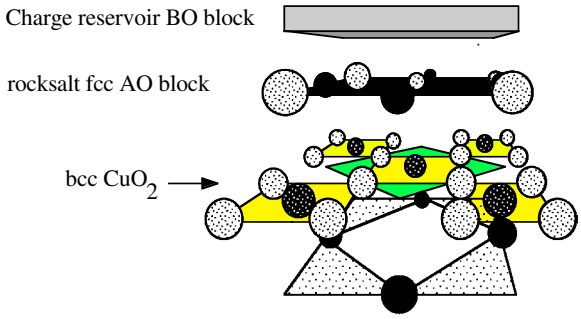

Figure 2. The heterostructure of a generic cuprate perovskite made of a superlattice of CuO_2, AO and BO oxide layers.

doping level should shed light on the pairing mechanism in cuprates, which remains unresolved even after 19 years from the discovery of high-T_c superconductivity in these materials.

2. The heterogeneous lattice of cuprates

The cuprate perovskites are heterogeneous materials formed by three different building blocks [BO](AO)CuO_2: the metallic bcc CuO_2 layers, the insulating AO layers (rock-salt fcc layers in hole doped cuprates) (A = Ba, Sr, La, Nd, Ca, Y, etc) and the charge reservoir BO layers as shown in figure 2. It is well known that the cuprate perovskite lattice is stable only up to a critical value of the lattice tolerance factor between the CuO_2 layer and the rocksalt layers [2, 3].

In hole (electron) doped superconductor the compressive (tensile) stress exerted on the CuO_2 plane by the lattice mismatch induces a compressive (tensile) CuO_2 strain of the Cu–O distance and a tensile (compressive) CuO_2 strain on the rocksalt layer. The different lattice mismatch or misfit between the building blocks of the different perovskites induces an internal pressure on the CuO_2 lattice modulating the Cu–O distance in the plane and the superconducting critical temperature [4–7]. This is in qualitative agreement with the experimental evidence that in doped La_2CuO_4 film T_c depends on the crystalline strain induced by the perovskite film induced by the lattice mismatch with the substrate [8, 9].

In a particular family $(La_{1-y}Nd_y)_{2-x}Sr_xCuO_4$ it was found that the superconducting phase is not simply controlled by x (controlling the hole doping) but also by y, controlling the structure of the undoped parent compound $(La_{1-y}Nd_y)_2CuO_4$ [10]. It was proposed that the average buckling of the CuO_2 layer (pushing the Cu–O–Cu bond angle away from 180°) measured by crystallography provides a second variable for the phase diagram of cuprate superconductors since the superconducting phase is suppressed by the onset of an insulating antiferromagnetic phase for a buckling angle ϕ larger than a critical value 3.6°. This electronic phase occurs in the low temperature tetragonal (LTT) CuO_2 lattice phase with a stable static magnetic charge and lattice one-dimensional ordering at doping 1/8 (called LTT stripe phase) [10–13]. In contrast, in other families with tetragonal lattice the average Cu–O–Cu deviates from 180° by a larger buckling angle 6.5° at optimum doping for superconductivity and a scaling of increasing buckling with increasing T_c has been found [14].

There is now increasing experimental evidence for textures at mesoscopic scale (in the range 1–20 nm) in the CuO_2 lattice that play an essential role in the onset of superconductivity with short coherence length. There is growing evidence that the striped lattice modulation of the CuO_2 plane in Bi2212 could be a key to understanding the mesoscopic lattice textures in more disordered cuprate perovskites. In fact, there are several reports on different stripe orders, observed by magnetic scattering studies, scanning tunnelling spectroscopy (showing local density of state modulations near the Fermi level), NMR and other probes [15]. The solution of the mesoscopic structure requires the use of local and fast probes and the analysis of weak and diffuse in x-ray diffraction line profiles beyond the average crystallographic peaks.

3. The local strain in the CuO_2 lattice

The Cu–O pair distribution function in the CuO_2 plane has been measured in different cuprate families by polarized Cu K-edge EXAFS [16–18], that is a fast (10^{-15} s) and local probe, via photoelectron single scattering processes. We have been able to identify the key role of the strain of the CuO_2 lattice to derive the superconducting temperature [19–23]. We have focussed on a set of perovskite families, where the hole doping is obtained by adding interstitial oxygen ions on the charge reservoir layers, and we have established the relation of the local chemical pressure acting on the CuO_2 layer with the local strain in the CuO_2 lattice and shown that it controls the superconducting critical temperature [19–24].

The average Cu–O distance as a function of the average ionic radius of the metal ions in the (AO) block layers in contact with the CuO_2 plane is plotted in figure 3. The non-superconducting cuprates show the Cu–O equilibrium distance $R_0 = 197$ pm. By decreasing the ionic radius the phase diagram of the lattice structure goes from the tetrahedral (T) phase of mercury-based cuprates (Hg1201, Hg1212) to the orthorhombic (O) phase (Bi2212 and La214). Decreasing the average ionic radius in the $(La_{1-y}Nd_y)_2O_2$ block of $(La_{1-y}Nd_y)_{2-x}Sr_xCuO_4$ system by increasing y, the system goes in the LTT phase for $x > 0.12$ or in the Pcnn phase for $x < 0.12$ where the buckling of the Cu–O–Cu bonds increases with decreasing the ionic radius $R_{(AO)}$ in the $(La_{1-y}Nd_y)_2O_2$ block layers due to an increasing compressive stress acting on the CuO_2 plane. Beyond a critical stress for the Nd content $y = 0.8$ the tensile stress acting on $(La_{1-y}Nd_y)_2O_2$ block induces a phase transition from rocksalt to fluorite type structure releasing the internal pressure and the perovskite shift to T′ structure of electron doped perovskites with the fluorite structure of the Nd_2O_2 blocks inducing a tensile stress on the CuO_2 layers.

The maximum superconducting critical temperature T_{cmax} for each cuprate family occurs at about the same doping level $0.15 < \delta_{optimum} < 0.18$ as can be seen in figure 1. We have

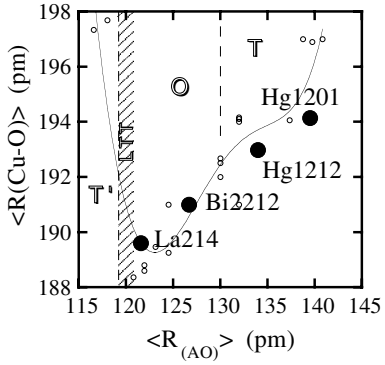

Figure 3. The copper–oxygen distance in plane R(Cu–O) as a function of the average ionic radius in the AO block layers $R_{(AO)}$.

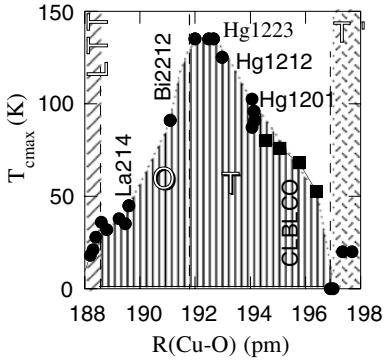

Figure 4. The critical temperature at optimum doping in different cuprate perovskite families as a function of the copper–oxygen distance in plane R(Cu–O), with the structural phase diagram showing the four different crystallographic structures tetragonal (T′ and T), orthorhombic (O) and pseudotetragonal (LTT). The hole doped $(Ca_xLa_{1-x})(Ba_{1.75-x}La_{0.25-x})Cu_3O_y$ (CLBLCO) family with tetragonal structure provides the case of superconducting hole doped perovskites with the largest Cu–O bonds.

plotted in figure 4 the values of T_{cmax} as a function of the Cu–O distance R. The systems where the Cu–O distance is at the equilibrium distance $R_0 = 197$ pm do not show superconductivity. The superconducting T_c increases with decreasing the Cu–O distance in the range 196–192 pm in tetrahedral systems reaching a maximum at around 192 pm. The critical temperature decreases with decreasing the Cu–O distance in the range 192–188 pm where the lattice shows a non-homogeneous orthorhombic structure. Both the tetragonal (T) low strain systems and the high strain LTT systems show an average buckling angle in the range of 3–6°. The systems in the orthorhombic phase show a modulated buckling angle Cu–O–Cu in the range of 2–16° as shown by EXAFS in La214 [17] and by both EXAFS [16] and x-ray anomalous scattering [25] in Bi2212. In particular, Bi2212 shows a striped lattice structure characterized by a 1D modulation of the Cu–O (apical) distance [26] related to the 1D modulation of the buckling of the CuO_2 lattice [25, 27] associated with a displacement of the Cu ion out of the plane of the coordinated oxygen ions (dimpling) that is modulated with a wavevector $Q_1 = 0.4(\pi, \pi)$, in units of $1/d$ where d is the Cu–O–Cu

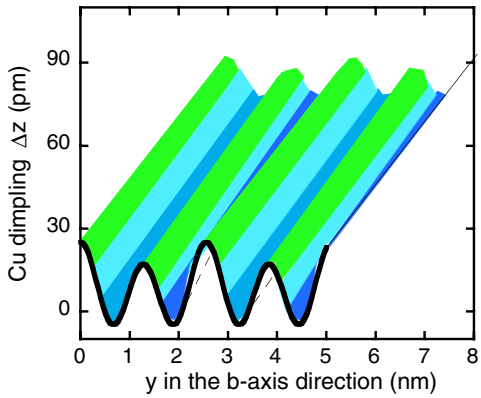

Figure 5. The dimpling of Cu ions out of the oxygen plane as a function of distance along the distance in the *b*-axis direction of the superstructure.

distance in the standard tetragonal notation, or $Q_1 = 0.4(2\pi/a_0)$ where $a_0 \sim d\sqrt{2}$ is the orthorhombic axis of the unit cell of Bi2212 or La214 as shown in figure 5. The anisotropy of the local structure at mesoscopic level has been determined by Cu-K edge EXAFS experiments [27]. The static structure of the Cu displacement (Δz) out of the oxygen plane by an order of 30 pm, that implies a modulation of the component of the Cu–O molecular orbitals with $ml = 0\,(3\mathrm{d}z^2 - r^2)$.

The evidence that the CuO_2 plane of a material in the orthorhombic phase is not homogeneous is provided by many experimental local probes, and the fact that the average electronic structure has neither the average tetragonal nor orthorhombic symmetry is clearly shown by the momentum scanning photoemission experiment in figure 6 [28]. The results of this experiment carried out at room temperature have been confirmed by Fretwell *et al* [29] at liquid He temperature as is shown in figure 7.

Figure 6 shows the distribution of the spectral weight of quasi-particles at the Fermi level (in the range of 50 meV around the Fermi level) as a colour plot as a function of the in-plane electron momentum $q(k_x, k_y)$. It is clear in the upper figure that the two orthorhombic high symmetry directions $X(-\pi, \pi)$ and $Y(\pi, \pi)$ as well as the two tetragonal high symmetry directions M1(π,0) and M2(0, π) are different. In the *Y*-direction the states at the Fermi level have a pure $d_{x^2-y^2}$ L(b_1) symmetry, therefore are fully suppressed by dipole selection rules in the first Brillouin zone (BZ), in our detection geometry called 'even symmetry'. This is confirmed by the fact that these $d_{x^2-y^2}$ L(b_1) are strong in the second BZ zone where the transition is allowed by dipole selection rules. In contrast, the states at the Fermi level at the crossing in the *X*-direction have a mixed symmetry (not pure $d_{x^2-y^2}$ L(b_1)), since they are only weakly suppressed by the dipole selection rule in the first BZ zone and are very weak in the second BZ. A clear difference is also observed between M1 and M2. The difference in the second BZ zone where the Fermi surface appears is open in the M2 direction (see figures 6 and 7), while it is more closed in the M1 direction. The anisotropy of the local structure between the *X*- and *Y*-direction has also been observed by polarized Cu K-edge EXAFS experiments [29].

The photoemission data show that the compressive strain of the Cu–O bonds induces a variation of the electronic structure. The data shown in figure 8 reveal that the hopping integral from Cu to oxygen increases with increasing ε as expected, but the variation is quite small. In contrast, the next near-neighbour integral t' giving the oxygen–oxygen hopping in the plane

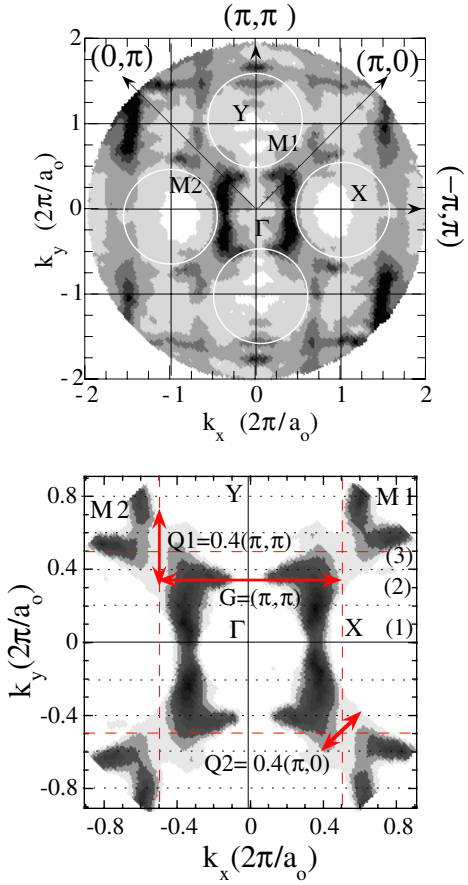

Figure 6. The Fermi surface determined by momentum scanning photoemission experiment. In the first Brillouin zone (enlarged in the lower panel) the dipole selection rule selects the states with even symmetry while in the second Brillouin zone the odd states are selected (see the upper panel). The circles in the upper figure indicate the expected Fermi surface. The wavevectors **G**, **Q**1 and **Q**2 connecting points of the Fermi surface where the quasi-particle spectral weight is suppressed (hot spots) are indicated in the lower panel.

shows an unexpected behaviour since it decreases with increasing strain and goes towards zero at a strain value of about 0.07.

4. The self-organization of pseudo-Jahn Teller (JT) polarons

There is growing evidence that the electron–phonon coupling is a key parameter for understanding the physics of the correlated electron fluid in cuprates. The non-conventional electron–phonon coupling and its relevance for understanding the physics of cuprates is indicated by several experiments [30–39] that have been interpreted in terms of an inhomogeneous phase at mesoscopic level where localized charges and itinerant charge coexist. The localized charges are trapped in regions of 6–8 copper sites forming polarons in the intermediate coupling regime and they get self-organized forming 1D arrays of polaron strings

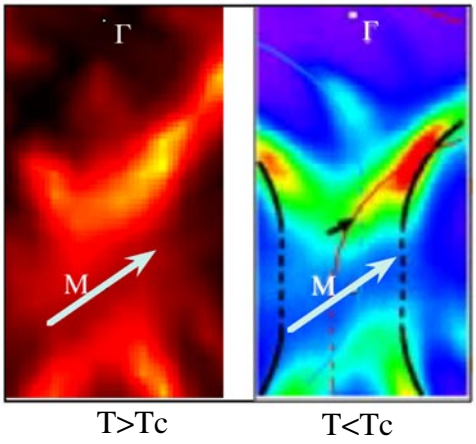

Figure 7. The momentum scanning photoemission data of the Fermi surface near the M2 point measured at $T = 300$ K by Saini *et al* [28] and at liquid helium temperature by Fretwell *et al* [29].

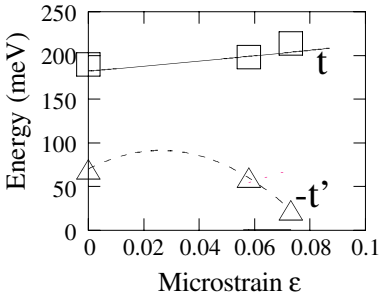

Figure 8. The near-neighbour hopping integral t (Cu–O) and the next near-neighbour integral t' (oxygen–oxygen) as a function of the microstrain ε in different cuprates.

or stripes [40–44]. The local lattice distortions and the orbital symmetry show that the polarons have a pseudo-Jahn Teller character [45, 46].

The self-organization in a striped pattern in a short mesoscopic scale of pseudo-Jahn Teller polarons is shown in figure 5. Recently, it has been shown that in orthorhombic oxygen doped La214 a mesoscopic texture is realized where a commensurate 3D charge ordering at doping 1/8 coexists with superconducting domains. This phase is accompanied by oxygen ordering in the temperature range below 350 K and it shows spin ordering below 40 K [47, 48].

5. The phase diagram of cuprate superconductors

The CuO_2 strain ε defined as $\varepsilon = 2(R(\text{Cu–O}) - R_0)/R_0$ (where R_0 is the unstrained Cu–O bond length, $R_0 = 197$ pm) has been shown [18–24] to be the second variable needed to define the phase diagram of cuprate perovskites, beyond doping δ. Figure 9 shows the location of the major families of cuprate superconductors in the plane (ε, δ). We can identify four regions characterized by the symmetry of the crystallographic lattice. In the first region (T), at low strain ($\varepsilon < 0.04$), the materials show a tetragonal structure. In the second region (O)

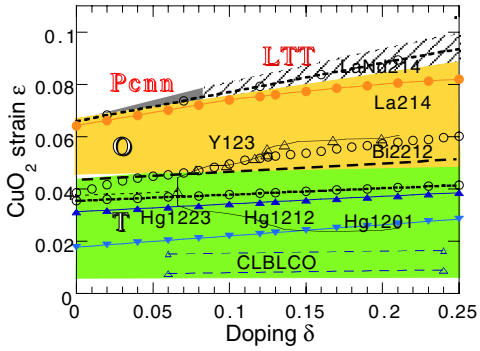

Figure 9. The (ε, δ) phase diagram for the cuprate superconductors showing different regions with different average crystallographic structures.

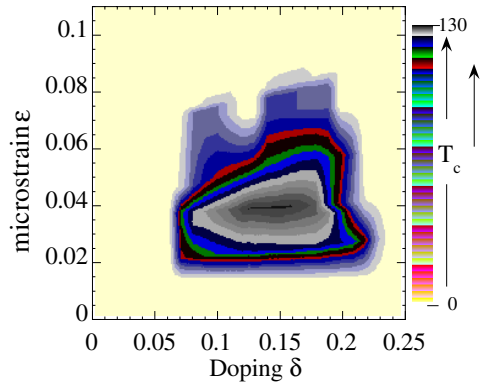

Figure 10. The phase diagram of the superconducting critical temperature $T_c(\varepsilon, \delta)$ plotted as a colour plot as a function of two variables (doping and microstrain).

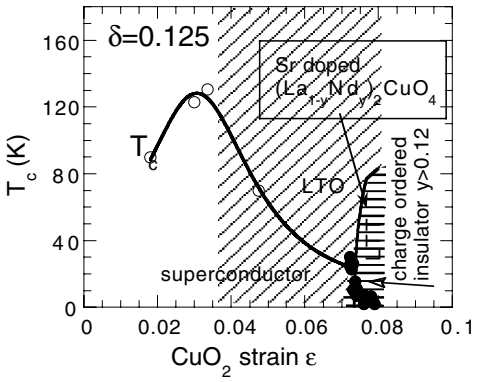

Figure 11. The variation of the superconducting critical temperature T_c as a function of the elastic local strain of the CuO_2 lattice at constant doping $\delta = 1/8$.

at intermediate coupling in the range ($0.04 < \varepsilon < 0.07$) the lattice shows different types of orthorhombic crystallographic structures. In the third region the lattice shows the Pcnn lattice

symmetry. In the fourth region the lattice shows the LTT lattice symmetry where the local distortion of the CuO_4 square plane is of the type predicted for pseudo-JT polarons. The $T_c(\delta, \varepsilon)$ represents a universal phase diagram in which the T_c reaches the highest value $T_c \approx 150$ K at $\delta_c \sim 0.16$, $\varepsilon_c \sim 0.04$ (figure 10). It is of particular interest to study the variation of the critical temperature T_c as a function of the strain ε at constant doping $d = 1/8 = 0.125$ that is shown in figure 11. The critical temperature reaches a maximum near $\varepsilon = 0.04$. At about $\varepsilon = 0.07$ it shows a sharp decrease associated with the phase transition from the LTO phase to the LTT phase shown in figure 11. The formation of the LTT crystallographic phase at doping $1/8$ goes together with the formation of a striped pattern of spin, charge and local lattice distortions.

Acknowledgments

This work is supported by 'progetto cofinanziamento Leghe e composti intermetallici: stabilità termodinamica, proprietà fisiche e reattività' of MIUR, and by 'Progetto 5% Superconduttività' of Consiglio Nazionale delle Ricerche (CNR).

References

[1] Bianconi A, Congiu Castellano A, De Santis M, Rudolf P, Lagarde P, Flank A M and Marcelli A 1987 *Solid State Commun.* **63** 1009
[2] Goodenough J B 1990 *Supercond. Sci. Technol.* **3** 26
Goodenough J B and Marthiram A 1990 *J. Solid State Chem.* **88** 115
[3] Rao C N R and Ganguli A K 1995 *Chem. Soc. Rev.* **24** 1
[4] Ihara H 1994 *Bull. Electrotech. Lab.* **58** 64
Also see e.g., Izumi F and Takayama-Muromachi E 1995 *High Temperature Superconducting Materials and Engineering* ed D Shi (Oxford: Pergamon) p 81
[5] Edwards P P, Peakok G B, Hodges J P, Asab A and Gameson I 1996 *High T_c Superconductivity: Ten Years After the Discovery (Nato ASI, vol 343)* ed E Kaldis, E Liarokapis and K A Müller (Dordrecht: Kluwer) p 135
[6] Marezio M and Licci F 1997 *Physica* C **282** 53, and references therein
[7] Attfield J P, Kharlanov A L and McAllister J A 1998 *Nature* **394** 157, and references therein
[8] Locquet J P, Perret J, Fompeyrine J, Machler E, Seo J W and Van Tendeloo G 1998 *Nature* **394** 453
[9] Sato H, Tsukada A, Naito M and Matsuda A 2000 *Phys. Rev.* B **61** 447
[10] Büchner B, Breuer M, Freimuth A and Kampf A P 1994 *Phys. Rev. Lett.* **73** 1841, and references therein
[11] Noda T, Eisaki H and Uchida S 1999 *Science* **286** 265
[12] Zhou X J, Bogdanov P, Kellar S A, Noda T, Eisaki H, Uchida S, Hussain Z and Shen Z X 1999 *Science* **286** 268
[13] Ichikawa N, Uchida S, Tranquada J M, Niemöller T, Gehring P M, Lee S-H and Schneider J R 2000 *Phys. Rev. Lett.* **85** 1738
Tajima S, Noda T, Eisaki H and Uchida S 2001 *Phys. Rev. Lett.* **86** 500
[14] Chmaissem O, Jorgensen J D, Short S, Knizhnik A, Echstein Y and Shaked H 1999 *Nature* **397** 45–8
Knizhnik A, Direktovich Y, Reisner G M, Goldschmidt D, Kuper C G and Echstein Y 1999 *Physica* C **321** 199–206
Goldschmidt D, Reisner G M, Direktovich Y, Knizhnik A, Gartstein E, Kimmel G and Echstein Y 1993 *Phys. Rev.* B **48** 532
[15] Bianconi A and Saini N L (ed) 2000 *Stripes and Related Phenomena* (New York: Kluwer/Plenum)
[16] Bianconi A, Saini N L, Rossetti T, Lanzara A, Perali A, Missori M, Oyanagi H, Yamaguchi H, Nishihara Y and Ha D H 1996 *Phys. Rev.* B **54** 12018
[17] Bianconi A, Saini N L, Lanzara A, Missori M, Rossetti T, Oyanagi H, Yamaguchi H, Oka K and Ito T 1996 *Phys. Rev. Lett.* **76** 3412
[18] Saini N L, Oyanagi H, Lanzara A, Di Castro D, Agrestini S, Bianconi A, Nakamura F and Fujita T 2001 *Phys. Rev.* B **64** 132510
[19] Bianconi A, Agrestini S, Bianconi G, Di Castro D and Saini N L 2000 *Stripes and Related Phenomena* ed A Bianconi and N L Saini (New York: Kluwer/Plenum) p 9

[20] Bianconi A, Bianconi G, Caprara S, Di Castro D, Oyanagi H and Saini N L 2000 *J. Phys.: Condens. Matter* **12** 10655
Di Castro D, Bianconi G, Colapietro M, Pifferi A, Saini N L, Agrestini S and Bianconi A 2000 *Eur. Phys. J.* B **18** 617
[21] Bianconi A 2000 *Int. J. Mod. Phys.* B **14** 3289
[22] Bianconi A, Saini N L, Agrestini S and Di Castro D 2000 *Int. J. Mod. Phys.* B **14** 3342
[23] Bianconi A, Agrestini S, Bianconi G, Di Castro D and Saini N L 2001 *J. Alloys Compounds* **317–318** 537
[24] Saini N L, Bianconi A and Oyanagi H 2001 *J. Phys. Soc. Japan* **70** 2092–7
[25] Bianconi A, Lusignoli M, Saini N L, Bordet P, Kvick A and Radaelli P 1996 *Phys. Rev.* B **54** 4310
[26] Bianconi A, Della Longa S, Missori M, Pettiti I and Pompa M 1992 *Lattice Effects in High-T_c Superconductors* ed Y Bar-Yam, T Egami, J Mustre de Leon and A R Bishop (Singapore: World Scientific) p 6
Bianconi A 1993 *Phase Separation in Cuprate Superconductors* ed K A Muller and G Benedek (Singapore: World Scientific) p 352
Bianconi A 1993 *Phase Separation in Cuprate Superconductors* ed K A Muller and G Benedek (Singapore: World Scientific) p 352, 125
Bianconi A, Della Longa S, Missori M, Pettiti I, Pompa M and Soldatov A 1993 *Japan. J. Appl. Phys.* **32** (*Suppl.* 32–2) 578
[27] Saini N L, Lanzara A, Bianconi A and Oyanagi H 2000 *Eur. Phys. J.* B **18** 257–61
[28] Saini N L, Avila J, Bianconi A, Lanzara A, Asensio M C, Tajima S, Gu G D and Koshizuka N 1997 *Phys. Rev. Lett.* **79** 3464
Saini N L, Avila J, Bianconi A, Lanzara A, Asensio M C, Tajima S, Gu G D and Koshizuka N 2000 *Physica* C **341–348** 2071
[29] Fretwell H M *et al* 2000 *Phys. Rev. Lett.* **84** 4449
[30] Bianconi A and Missori M 1994 *J. Phys. I France* **4** 361
[31] Zhou J-S and Goodenough J B 1997 *Phys. Rev.* B **56** 6288
[32] Muller K A, Zhao G-M, Conder K and Keller H 1998 *J. Phys.: Condens. Matter* **10** L291
[33] Bozin E S, Billinge S J L, Kwei G H and Takagi H 1999 *Phys. Rev.* B **59** 4445
[34] McQueeney R J, Petrov Y, Egami T, Yethiraj M, Shirane G and Endoh Y 1999 *Phys. Rev. Lett.* **82** 628
[35] Sharma R P, Ogale S B, Zhang Z H, Liu J R, Wu W K, Veal B, Paulikas A, Zhang H and Venkatesan T 2000 *Nature* **404** 736
[36] Lanzara A, Zhao G-M, Saini N L, Bianconi A, Conder K, Keller H and Müller K A 1999 *J. Phys.: Condens. Matter* **11** L541
[37] Rubio Temprano D, Mesot J, Janssen S, Conder K, Furrer A, Mutka H and Müller K A 2000 *Phys. Rev. Lett.* **84** 1990
[38] Hofer J, Conder K, Sasagawa T, Zhao G-M, Willemin M, Keller H and Kishio K 2000 *Phys. Rev. Lett.* **84** 4192
[39] Lanzara A *et al* 2001 *Nature* **412** 510
[40] Bianconi A 1994 *Solid State Commun.* **91** 1
[41] Bersuker G I and Goodenough J B 1997 *Physica* C **274** 267
[42] Kusmartsev F V 1999 *J. Physique* IV **9** Pr 10–321
[43] Kusmartsev F V 2000 *Phys. Rev. Lett* **84** 530, 5026
[44] Kusmartsev F V 2000 *Int. J. Mod. Phys.* B **14** 3530
[45] Bianconi M, Pompa A, Turtu S, Pagliuca S, Lagarde P, Flank A M and Li C 1993 *Japan. J. Appl. Phys.* **32** (*Suppl.* 32–2) 581
[46] Seino Y, Kotani A and Bianconi A 1990 *J. Phys. Soc. Japan* **59** 815
[47] Di Castro D, Colapietro M and Bianconi G 2000 *Int. J. Mod. Phys.* B **14** 3438
[48] Kusmartsev F V, Di Castro D, Bianconi G and Bianconi A 2000 *Phys. Lett.* A **275** 117